Journal of Advanced Scientific Research
Available online through https://sciensage.info

ISSN
0976-9595
Research Article

HIGHLY LUMINESCENT CU DOPED SNO$_2$ NANOCOMPOSITES AND THEIR PHOTOCATALYTIC APPLICATION AS EXCELLENT METHYLENE DYE REMOVAL

Sangar Begzaad, Jyoti Bala Kaundal, YC Goswami*
Nano Research Lab, School of Sciences, ITM University Gwalior, AH 43, Jhansi Road, Turari, Madhya Pradesh, India
**Corresponding author: ycgoswami@gmail.com, sangar.begzaad@gmail.com*

Received: 06-02-2022; Revised: 07-05-2022; Accepted: 14-05-2022; Published: 31-05-2022

https://doi.org/10.55218/JASR.202213417

ABSTRACT

Cu doped SnO$_2$ nanostructures were grown using hydrothermal method. The solution was obtained by dissolving stannous chloride in distilled water (DW) with ammonium as surfactant followed by irradiation with ultrasonic vibrations. Obtained samples were characterized by structural, morphological and optical studies. All the peaks in the X-ray diffractograms are identified and indexed as structure. In pure form of Cu nanoparticles shows crystalline structures and in high concentration of Cu in SnO$_2$ nanoparticles shows the disappearing of peaks occurring as the pH increases. Negative slope of Williamson–Hall plots indicates compressive strain. Particle size of Cu doped SnO$_2$ nanostructures decreases with increasingthe doping concentration. An optical study shows good luminescence in visible region. A strong quantum effect was evident from the far blue shifted optical direct and indirect band gap. 80% of MO dye removed from waste water.

Keywords: Nanocomposites, Hydrothermal, Photocatalytic, Luminescence, SnO$_2$, Copper, Methylene, Dye.

1. INTRODUCTION 05

Metal oxides are considered as basis of smart and functional materials that represent particular properties and diverse technological applications. Metal oxide semiconductors (MOSs), owing to their unique physical and chemical properties and diverse potential of applications such as nanoelectronics, optoelectronics, photonics devices, spintronics devices, storage devices and as catalysts, have attracted extensive research interests[1]. SnO$_2$, ZnO, TiO$_2$, CuO, NiO and Fe$_2$O$_3$ are examples of metal oxide semiconductors. Tin dioxide (SnO$_2$), also called Stannic oxide, is direct band gap and an n-type semiconductor with a large band gap of (3.6 eV at 300 K)[2,3]. It is an outstanding metal oxide due to its exclusive high optical transparency, high carrier density, high dielectric constant and remarkable chemical, mechanical and thermal stability [3-6]. Its spectacular properties have made it widely suitable for diverse applications such as flat-panel displays, liquid crystal display, touch sensitive screens, light emitting diodes, transparent conductive electrode, solar cells, photovoltaic cells, photodetector, protective coating, magnetic storage media, high-density energy storage material, rechargeable lithium-ion battery, sensors, photocatalysts and oxidation catalyst [4, 7-10].

Many methods are developed for the synthesisof either doped or undoped SnO$_2$ nanostructures namely, spray pyrolysis [11], hydrothermal methods [12], polymer precursor [13], evaporating tin grains in air [14], chemical vapor deposition [10], thermal evaporation of oxide powders [15], microwave-assisted solvothermal [16], magnetron sputtering [17], Sonochemical [18], VLS method [19], laser ablation [20], rapid oxidation of elemental tin [21] co-precipitation method [22] and sol-gel method [23]. By doping SnO$_2$ with transition metals, the optoelectronic properties such as photo-luminescence and optical band gap of SnO$_2$ is enhancing [24]. Chemical doping not only effect on the conduction band but also tailors the optical band gap of SnO$_2$ thin films [25, 26]. Doping SnO$_2$ with the transition metal ions (Fe, Mn, Cu, Ni, Co, Zn. etc.) in order to manipulate its properties is reported in recent literatures [27].

Based on reports, researchers have dopped SnO$_2$ with different metals and semiconductors for the diverse applications purposes due to potential inherent properties of SnO_2. In this study, we only focus on Cu dopped SnO_2 literature. Reports show that, surface area of the SnO_2-based powders are increasing while additive (metal cations: Al, Co, Fe and Cu) are added [28]. Pure SnO_2 nanoparticles are dopped with the Cu and Ni using co-precipitation method and the structural, morphological, optical, magnetic and electrical properties of the grown material is studied [29]. Co-precipitation, compared to other methods, is reported as novel economical technique with a large-scale production possibility, low cost, high sample purity, particle surface customizability, low pressure and temperature, and chemical homogeneity method. SnO_2 thin films, with different Cu doping concentrations, is prepared by spray pyrolysis method [30]. Gong Zhang et al. have used sol-gel method for doping SnO_2 powder with CuO as dopant for the gas sensor applications [31] and 9 wt.% of Cu in SnO_2 by solvent evaporation method is reported by More et al. and its gas sensing behavior is studied at different annealed temperature [32]. Hu et al., from the effect of Cu and Rh on the optical properties of tin dioxide, have inferred that effective localization of free electron at the surface defects of host material of Cu is more that Rh as dopant [33]. Using chemical precipitation method, SnO_2 and Cu doped SnO_2, with two 10 and 20 wt.% concentration of Cu, is obtained [34]. Cu and Co doped tin dioxide nanoparticles is prepared by simple co-precipitation technique and the effects are studied extensively [35]. The variation results of structural, photoluminescence and gas sensing aspects of SnO_2 due to Cu doping is analyzed by Mishra et al. [24] and Room Temperature Ferromagnetism (RTFM) property of Cu doped SnO_2 nanowire, grown on the silicon substrate by the thermal evaporation method and at atmospheric pressure, is reported by Johari et at. [36]. The reason for the origin is concluded that, the RTFM in Cu doped SnO_2 nanowire is due to surface defects and oxygen vacancy. SnO_2 thin films with high work function and wide band gap has a significant impact on its application on optoelectronic devices and based on report, Cu as dopant of SnO_2 increases the work function of the SnO_2 thin films [37]. Cu doped SnO_2 thin films, using spray pyrolysis methodis reported, as well[30]. Cu-doped SnO_2 Nanosheet Arrays (Cu- SnO_2 NSAs), by a single step homogeneous precipitation method, is reported [38].

Photocatalytic technologies, which are eco-friendly, show many environmental potential applications. Among others, semiconductor-based photocatalysts are reported for organic degradation, water treatments, heavy metal ions reduction, and CO_2 reduction [39-40]. SnO_2 is early used for photocatalytic applications by M.S. Wrighton in 1976 [39]. SnO_2 due to high oxidation potential and chemical inertness, long-term stability, non-toxicity, cost-effective, and eco-friendly, has gained large research interests [41-42]. However, the pristine SnO_2 photocatalytic properties are far from practical application owing to the drawbacks: large bandgap (3.6 eV) that only UV spectrum range absorption is possible, and serious electron-hole pairs recombination [39]. To resolve this challenge, the bandgap can be tailored. In order to adjust the bandgap, one possible route is to dope the SnO_2. In this study, we dope SnO_2 with copper (Cu) by hydrothermal method in order to study the photocatalytic properties for different dye degradation applications.

2. MATERIAL AND METHODS

2.1. Material

Cu doped SnO_2 powder was obtained by hydrothermal method. For the Cu doped SnO_2 nanoparticles synthesis, Stannous Chloride ($SnCl_2.{}_2HO$ =225.63), Cuprous Chloride (CuCl = 99), Distilled Water and Liquid Ammonia (NH_3) as catalyst, were used as precursors. All the chemical materials used in this experiment were of analytical grade and used without any further purification. Moreover, the glass vessels were cleaned using chromic acid and distilled ware by multiple steps.

2.2. Method

Initially, 0.1M of $SnCl_2.2HO$ was dissolved in 100ml distilled water. Similarly, 0.1M of CuCl was dissolved in 100ml of distilled water. Both samples were stirred at 10ºC ($SnCl_2.2HO$) and 60ºC (CuCl) continuously for 3 hours. Different ratios of SnO_2:Cu (0:1, 1:0, 1:1, 1:1.5, 1.5:1, 1:2.5, 2.5:1) were made in individual beakers. Then 5 drops of liquid ammonia (NH_3) were added to each ratio. First sample was kept in ppl lining autoclave reactor and placed in oven at temp 150°C for 2 hours. The autoclave reactor was cooled and filtered at room temperature and obtained particles werewashed with distilled water and acetone. Same process was repeated for all the samples.

2.3. Chemical Equation

$$SnCl_2.2H_2O + H_2O \xrightarrow{10^{\circ}C} SnO_2\,(S) + 2HCl\,(aq) + H_2O$$

$$CuCl + H_2O \xrightarrow{60^{\circ}C} CuO\,(s) + HCl\,(aq)$$

$$3CuO + 2NH_3 150^{\circ}C \longrightarrow 3Cu\,(s) + N_2\,(g) + 3H_2O$$

$$SnO_2\,(s) + Cu\,(s)\ 150^{\circ}C \longrightarrow SnO_2Cu$$

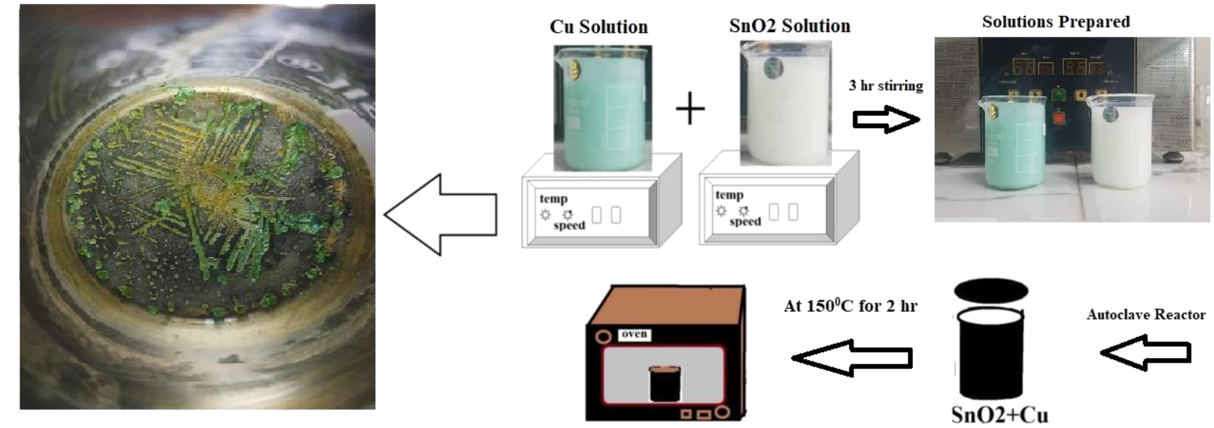

Cu-doped Tin Oxide Nanocomposites In Rod Shaped

Fig. 1: Cu doped SnO_2 synthesis method using hydrothermal method. Self-assembled wire shape structures visible by naked eyes are obtained.

2.4. Photocatalytic experiment

The photocatalytic activity of Cu doped SnO_2 nanocomposites was calculated for the methyl orange (MO) dye under the sunlight. The chemical formula of methyl orange in Fig. 2.

All the experiments werecarried under sunlight at ITM University, Gwalior in equal interval of time. For this experiment, 40 ppm of dye solution was prepared in the lab and 0.5g of photocatalyst was added in the dye solution. All the readings of adsorption-desorption were carried at 464nm wavelength in the time interval from t=0 to t=150 minutes.

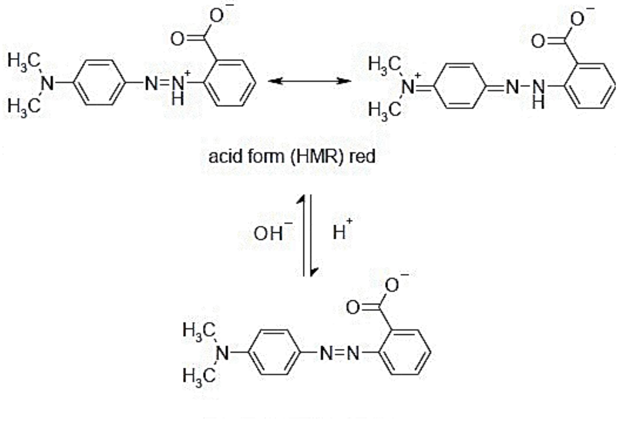

Fig. 2: Chemical formula of methyl orange

2.5. Characterization Techniques

The obtained powder was characterized by Fourier Transformation Infrared (FT-IR), UV-Visible spectroscopy and Photoluminescence (PL) spectroscopy. X-ray diffractograms were obtained in the in the angle of 2 theta ranging from 2 to 90 with Cu $k\alpha$ radiation of wavelength 1.54 nm using Mini Flex 350/650 XRD.FT-IR Spectroscopy analysis was carried out by Perkin Elmer spectrophotometer using dispersive mode. All the samples were analyzed within wavenumber region of 4500 to 500 cm^{-1}. For the optical studies, UV-Visible optical absorption was carried out by Perkin lambda 25 and Photoluminescence (PL) studies was carried out by Perkin Elmer LS-55.

3. RESULTS AND DISCUSSION

3.1. Structural Studies (X-Ray Diffraction)

In fig.3, X-ray diffractograms for SnO_2/Cu doped nanoparticles with various SnO_2 and Cu concentrations are shown. the JCPDS file (card No: 41-1445) shows the presence of SnO_2 nanoparticles of tetragonal positions and therefore the JCPDS file (card No:85-1326) shows the presence of Cu nanoparticles. However, with increasing concentration of Cu in SnO_2 the sharpness of peaks decreases. Diffractogram for Cu show (111), (200), (220) planes verified with the JCPDS file (card No: 85-1326) and crystals planes (101), (200), (220),(221), and (002) corresponds to SnO_2nanoparticles which shows the presence of SnO_2 nanoparticles of tetragonal geometry.

The average nano-crystallite size (D) was calculated using the Scherrer formula,

$$D=0.9\lambda/\beta \mathrm{Cos}\theta \qquad (1)$$

Where, λ is that the X-ray wavelength, θ is that the Bragg diffraction angle, and β is that the FWHM of the XRD peak appearing at the diffraction angle θ. The crystalline sizes were estimated from the Scherer's relation and therefore the size decreases or increases on doping of copper in SnO_2 nanoparticles. It indicates that a rise within the doping concentration of Cu in tin oxide decreases the typical crystalline size. On the opposite side, if Cu concentration is low then the dimensions increases. Table 1 shows the calculated values of the dimensions of SnO_2: Cu nanoparticles.

Micro strain of crystals were calculated by using Williamson halls plots. The graph plot between βCosθ and 4*Sinθ given in fig.3(b). Sample 1 and sample 5 showedtensile strengthand other samples have compressive strain and due to quenching effect, the intensity and peaks of samples disappears.

Table 1: The calculated value of the dimensions of SnO_2:Cu nanoparticles

Sample	FWHM	D=kλ/βCosθ	Intercept	Strain
Sample1	0.015403	112nm	-0.0115	0.01582- tensile
Sample2	0.0228	73.3	0.04703	-0.0167
Sample3	0.0287	55.4	0.03782	-0.00724
Sample4	0.4725	36.3	0.068	-0.01
Sample5	0.02241	75.7	0.012	0.005
Sample6	0.03558	46.4	0.05943	-0.01526

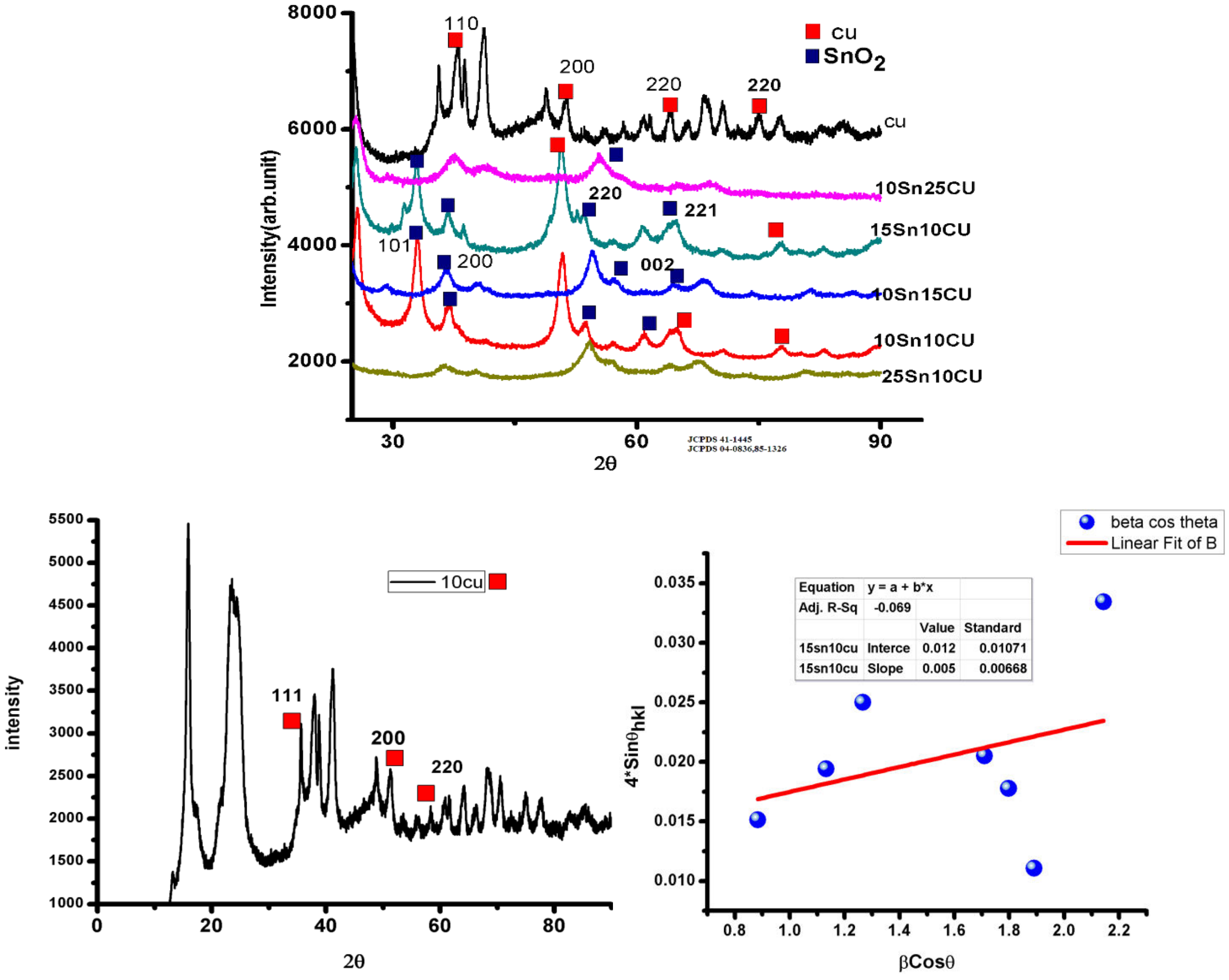

Fig. 3a: X-ray diffractograms for SnO_2/Cu doped nanoparticles with various SnO_2 and Cu concentrations.

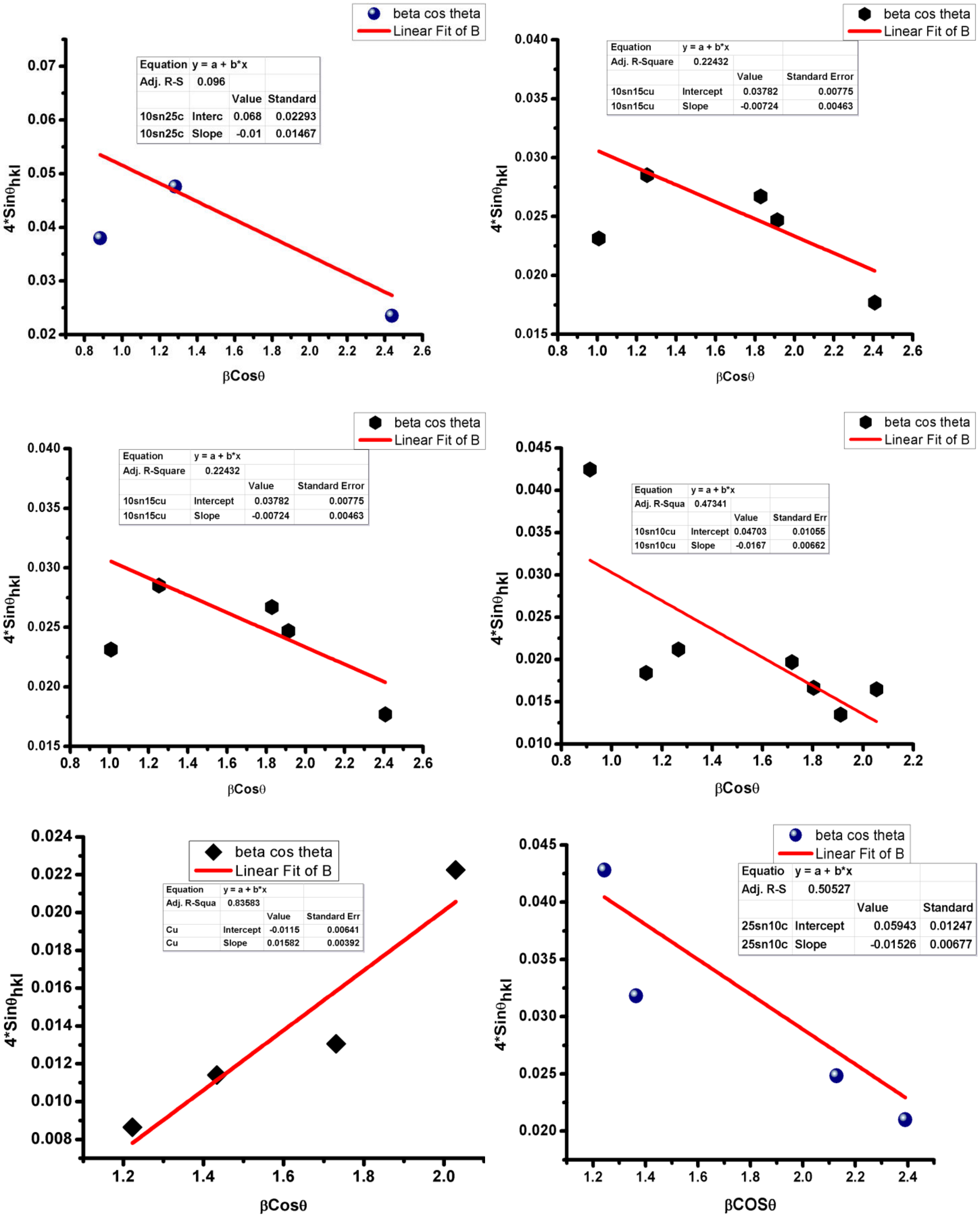

Fig. 3b: X-ray diffractograms for SnO_2/Cu doped nanoparticles with various SnO_2 and Cu concentrations.

3.2. Fourier Transformation Infrared (FT-IR) Studies

FT-IR spectral analysis was performed to confirm the chemical structure of all of the SnO_2 and copper doped composites. Fig.4 summarizes the FT-IR spectra of SnO_2 and copper doped nanopowder acquired in ATR Mode. FTIR is any Fourier Transform Infrared spectroscopy method in any measuring geometry, may it be transmission or reflection. ATR stands for Attenuated Total Reflection and is developed in order to enhance the surface sensitivity since IR spectroscopy is a bulk method. Table 2 shows all peaks assigned by SnO_2/Copper dopped samples. The FTIR spectrum is sensitive to functional groups. The vibration bands observed are at 3358 cm^{-1}, 3326 cm^{-1}, 3325 cm^{-1}, 3285cm^{-1}, 3343 cm^{-1}, 3321 cm^{-1} and 3344 cm^{-1} are attributed to O-H stretching vibrations. The peaks obtained at low frequencies 702 cm^{-1},706 cm^{-1}, 709 cm^{-1} and 718 cm^{-1} are due to the Cu-O vibrations. The broadband and weak peaks at about 2933 cm^{-1} are correlated to the presence of the O-H group while the bands at 1730 $cm^{-1}$and 1465 cm^{-1} are the standard vibration bands of C=O and C-O respectively. The band at 1580 cm^{-1} is additionally associated with C-C stretching. A band associated with symmetric and asymmetric vibrations of the C-O-C group is observed at 1150 $cm^{-1}$to 1300 cm^{-1}. The peaks above 1300 $cm^{-1}$to 1500 cm^{-1}shows C=O and O-H vibrations. Peak associated with Sn-O vibrations is observed from 650 cm^{-1} to 450 cm^{-1}. The intensities of peaks decrease or increase with the addition of Cu and Sn ratios within the samples.

Table 2: FTIR peaks assignments of the Cu doped SnO_2 nanoparticles

Sample Assignment	0Sn10Cu	10Sn0Cu	10Sn10Cu	10Sn15Cu	15Sn10Cu	10Sn25Cu	25Sn10Cu
Sn-O stretching vibrations	495	478	493	440,496	493	445,448	488,506
Sn-O/Cu –o bending vibrations	520,646	532,647	524,648	515,651	528,648	530,540,645	533,545,650
Cu	706,773,718	708	707	709	709	706	702,
CH_2 vibrations	912,996,1067	758,992	772,920,998	763,918,1073	769,849,925,998,1078	751,806,851, 922,996,1061	913,1013,1076,761
vibrations	1105,1215	1066,1107	1075	1116,1217	1103,1227	1103,1219	1104
Asymmetric stretching of carboxylic due to C=O, OH	1387	1350	1118,1207	1399,1380,1345	1391	1350,1339	1353,1396,
NH stretching vibrations	1412	1407	1351	1463	1401	1411	1403
C=O	1584	1598	1599,1602	1588	1598	1603	1605
OH	3358,2933	3326,2931	3325,2932,2826	3285,2981,2792	3343,2939,2879	3321,2922,2770,2698	2933,2800,3344,2707

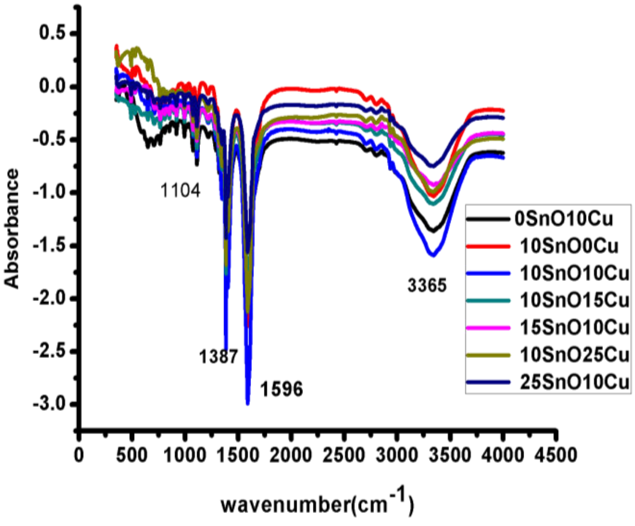

Fig. 4: FTIR spectra of nanocomposites of Cu doped SnO_2.

3.3. UV-Spectroscopy

The general equation of Tauc plot method is given by,

$$(\alpha h\nu)^{n} = K(h\nu - E_g) \quad (2)$$

Here "α "is the absorption coefficient, "$h\nu$ "is the incident photon energy, "K" is an energy independent constant and it is a parameter that depends on the transition probability, "E_g" is the bandgap energy and "n" is the nature of transition. In other words, n is a number characterizing the transition process which may take values: n = 2 for direct allowed transition, n= 1/2 for indirect allowed transition, n = 2/3 for forbidden direct transition and n = 1/3 for forbidden indirect transition.

The UV-vis Absorption spectra (Fig.5a) is obtained for SnO_2 and copper doped tin dioxide powder samples in the region 550-800 nm. It reveals that, almost all the samples show good absorption in the visible range.

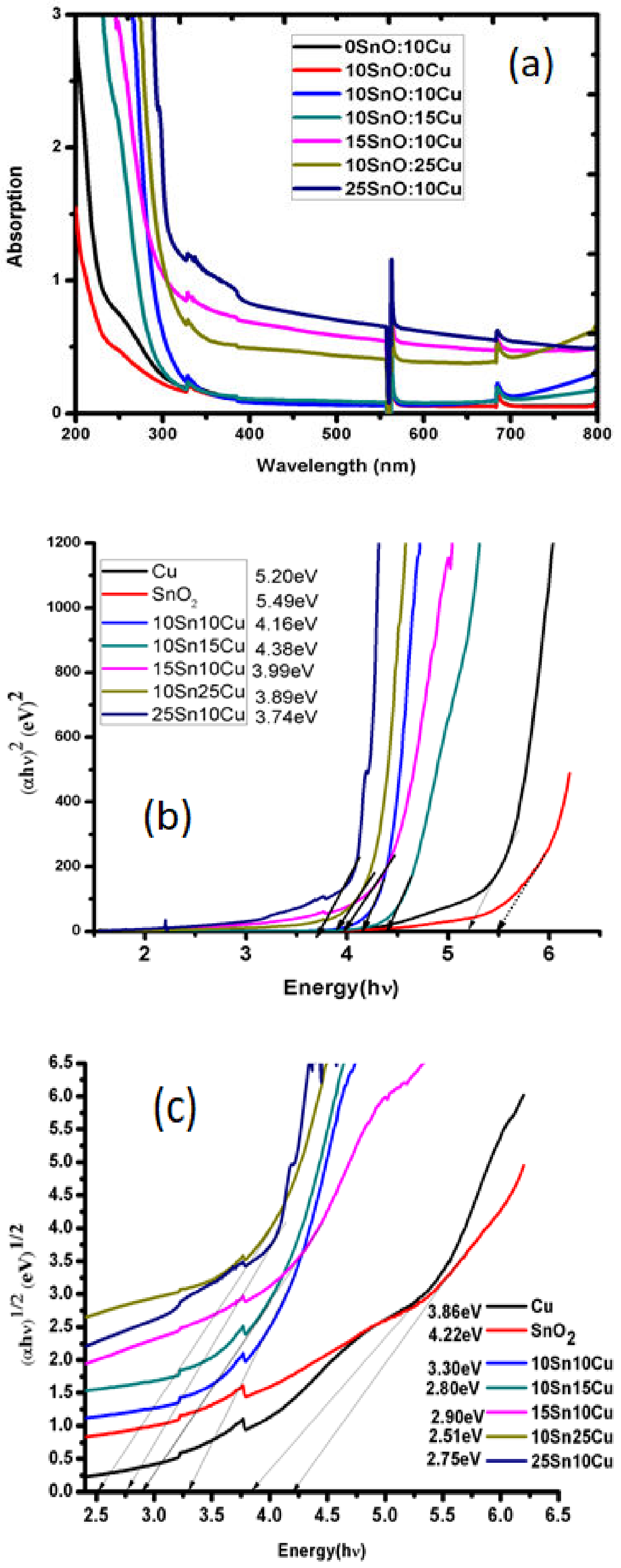

Fig. 5: The UV-Visible spectroscopy (A) Absorption peaks of samples and (B) The Tauc plot between energy and $(\alpha h\nu)^2$ (C) Indirect bandgap

The plot of (alpha hv)^2 vs. h*v* is shown in Fig. 5b. The bandgaps obtained for all the samples were ranging from 3.4 to 5.5 eV. Although there has been an appreciable change in SnO_2-to-Cu ratio with the variation of concentration, surprisingly, much variation is observed in band gap. This fact indirectly supports that, for SnO_2 there has been abruptly change in band gap. Furthermore, the indirect bandgap is obtained as shown in Fig.5c. The obtained indirect bandgap varies with different Cu concentration and it ranges within 2.51 to 3.3 eV. By Cu concentration increment in SnO_2, it results in decreasing the SnO_2 indirect bandgap.

3.4. Photoluminescence (PL) Studies

Based on the Fig.6, the SnO_2 has a broad luminescence peak from300 to 600nm in visible region and broad peak at higher wavelength from 450nm to 700 nm. Cu shows broad peak from 500nm to 700 nm in visible region. On increasing the doping of Cu in SnO_2 the intensity of PL peaks increases and shifted towards higher wavelength and small narrow peaks from 600 nm to 650 nm. This means it shows good luminescence behavior in visible region and formed small energy bands in SnO_2:Cu composites. Furthermore, it increases the time of recombination of holes and electrons.

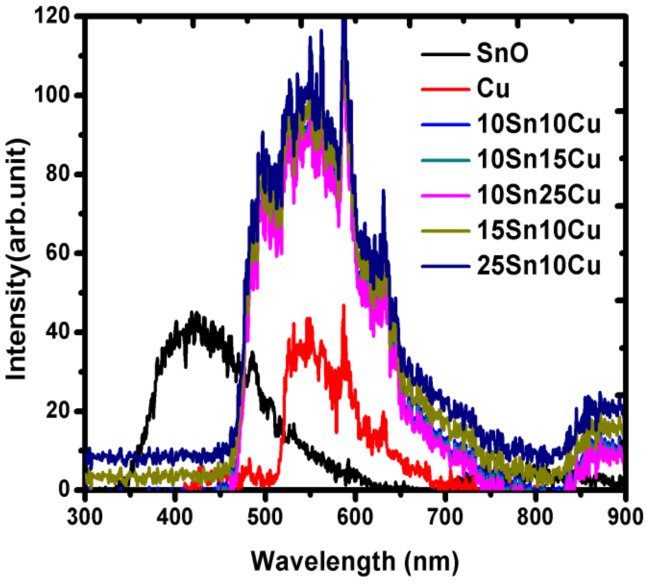

Fig. 6: The PL peaks of (A) SnO2 (B) Cu (C) 10SnOCu10 (D) 15SnOCu10 (e) 25SnOCu10

3.5. Photocatalytic studies

The photocatalytic activity were carried on MO dye with the Sample (a)SnO–Sample1 (b) Cu-Sample2 (c)

SnCu- Sample3 (d) Sn25 Cu Sample-4 (e) SnCu25-Sample 5.

The Fig. 7A shows the absorption of the curves of dyes when photocatalyst is present in the dye solution. The maximum absorption of dye solution was 5.1 at observed at 464nm. Pure SnO_2photocatalyst shows low degradation curve than Cu doped SnO_2photocatalyst; therefore, the Cu doping increases the rate of reaction. The variations occur in degradation curve is due the doping materials and increases the rate of recombination rate of electrons and holes. These electrons and holes react with the dye solution and degrade from the water. The concentration of dyes decreases with the coulombs force or attraction between dye and photocatalyst. vRate of concentration with time graph is shown in Fig. 7B.

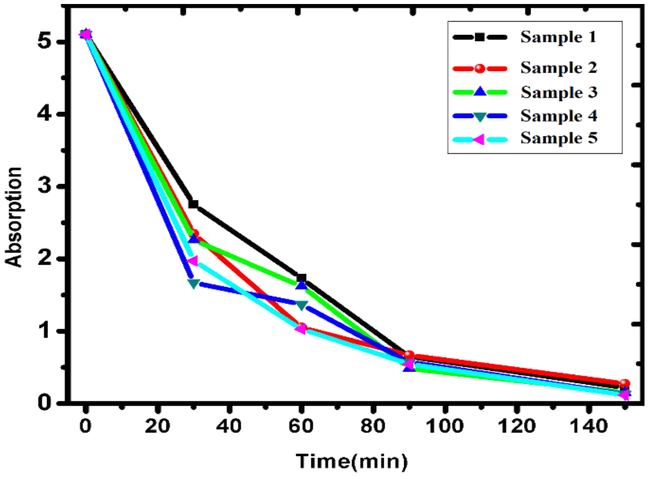

Fig. 7 (A): Absorption curve of Methyl orange in the presence of photocatalyst in sunlight

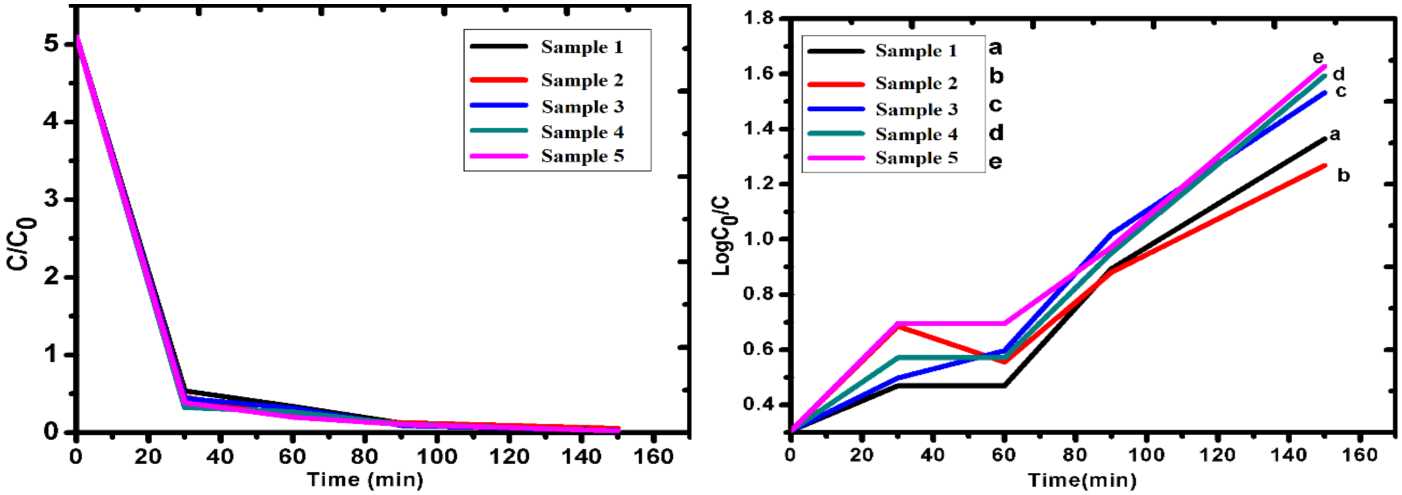

Fig. 7 (B): C/C_0 with time and Fig. 7(c). Log C_0 /C with time Curve of Methyl orange in the presence of photocatalyst (A) Sample1 (B) Sample2 (C) Sample3 (D) Sample4 in sunlight

3.5.1. Kinetic studies

Photocatalytic experiment values are calculated by using the Langmuir-Hinshelwood Kinetics model equation:

$\ln (C/C0) = Kt$ (3)

$k = \ln (C/C0)/t$ (4)

where,*kt* is the pseudo first-order rate constant (min^{-1}), C_0 is the initial concentration of dye, and C is the concentration of dye at time (t) respectively. The rate constant order of photocatalyst activity is as follows:

Sample1 > Sample2 > Sample3> Sample4> Sample5

The results clearly shows that the sample 4 compared to others samples has obtained excellent photocatalytic degradation activity of Methyl orange. As the Cu concentration increases in SnO_2 it provides the highest specific surface area. Sample 4 has more active sites of reaction for the Methyl orange degradation reaction. The degradation percentage of samples is calculated by above first equation. The degradation percentage graph is represented in the Fig. 8.

3.5.2. Mechanism of photocatalyst reaction

The proposed photocatalytic activity mechanism is shown in Fig. 9. When photon energy is greater than or equal to the bandgap energy of SnO_2 stimulates a valence band (VB) electron to the conduction band (CB) and producing a positive hole in the VB. The produced holes in VB are trapped by H_2O and produce hydroxyl radicals on the surface of SnO_2 and the electrons react with the oxygen molecules present in environment and generates the superoxide ions and then react with the water and converts to hydrogen peroxide and then converts the OH* radical. The number of hydroxyl is responsible for the degradation of particles.

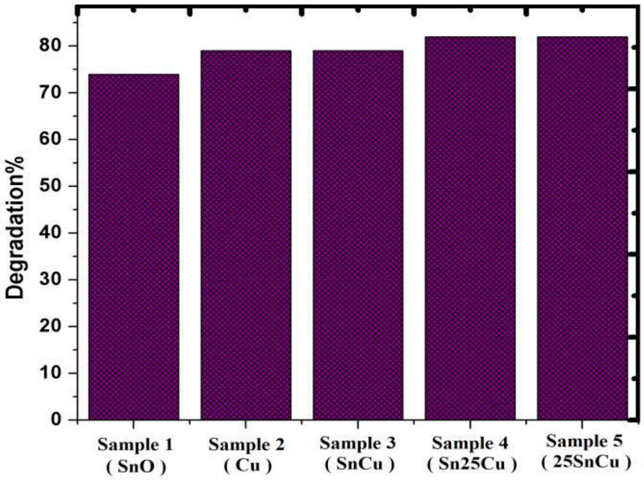

Fig. 8: Degradation percentage graph

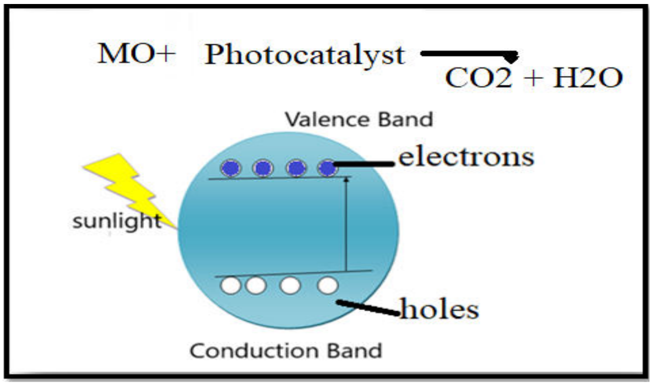

Fig. 8: Electron excitation representation diagram

4. CONCLUSION

In this study Cu doped SnO_2 nanopowder is synthesized using hydrothermal method. Growing from a salt mixture, we obtained SnO_2 and Cu nanocomposites with various copper contents. XRD studies indicated that with increasing concentration of Cu in SnO_2, the sharpness of peaks decreases. Moreover, the diffractogram showsthe planes verified for Cu and crystals planes correspond to SnO_2nanoparticles which show the presence of SnO_2 nanoparticles of tetragonal geometry. A rise within the doping concentration of Cu in tin oxide decreases the typical crystalline size but if Cu concentration is low then the dimensions increases.

The FTIR spectra revealed the conformation of SnO_2: Cunanocomposite. The intensities of peaks decrease or increase with the addition of Cu and Sn ratios within the samples. From other hand, the PL studies reveals that, on increasing the doping of Cu in SnO_2 the intensity of PL peaks increases and shifted towards higher wavelength and small narrow peaks from 600 nm to 650 nm. This means it shows good luminescence behavior in visible region and formed small energy bands in SnO_2:Cu composites. Furthermore, it increases the time of recombination of holes and electrons which is an important factor for photocatalytic applications. SnO_2 doping with Cu shifted the absorption edge to the lower energies because of the formation of SnO_2/Cu. Prolonged holding of the composite in water during salt matrix dissolution reduces the UV luminescence peak and gave rise to strong defect related luminescence in the green spectral region. There has been an appreciable change in SnO_2-to-Cu ratio with the variation of concentration and much variation is observed in band gap. The band gaps obtained for all the samples were ranging from 3.4 to 5.5 eV. Band gap decreases on increment of the Cu concentrations in SnO_2 composites. The obtained indirect band gap varies with different Cu concentration and ranges within 2.51 to 3.3 eve. It reveals that, by Cu concentration increment in SnO_2, it results in decreasing the SnO_2 indirect band gap.

Due to high band gap and good luminescence behavior in visible region, high time of recombination of holes and electrons; the Cu:SnO_2 composite has great potential application in photocatalytic reaction such as; photocatalytic hydrogen generation, water treatment, pollutants degradation, solar cell and also for Transparent conducting (TC) films. The Cu:SnO_2 could be hybridized with rGO for TCF purposes. In photo catalytic test carried on the methyl orange dye,it showed that high Cu in SnO_2particles shows good degradation effect. Inpure form 80% degradation percentage recorded after 150 min in sunlight.

5. ACKNOWLEDGEMENT

Authors are thankful to P C Ray center of research, ITM University Gwalior for providing characterizations facilities like UV-Vis spectroscopy, PL FTIR. Authors are also thankful to Central Instrumentation facilities, Jiwaji University Gwalior for providing X ray diffraction studies.

Conflict of interest

No conflict of interest

6. REFERENCES

1. Pascariu P, Airinei A, Grigoras M, Fifere N, Sacarescu L, Lupu N, et al. *Journal of Alloys and Compounds*, 2016; **68:**65-72.

2. Sharma R, Kumar V, Goswami YC. *Chalcogenide Letters,* 2021; **18(8):**473-479.
3. Sakthiraj K, Balachandra kumar K. *Journal of Magnetism and Magnetic Materials,* 2015; **395:**205-212.
4. Pan SS, Ye C, Teng XM, Li GH. *Journal of Physics D: Applied Physics*, 2007; **40(16):**4771.
5. Pan ZW, Dai ZR, Wang ZL. *Science*, 2001; **291 (5510):**1947-1949.
6. Wang B, Luo PG, Tackett II KN, Ruiz ON, Bunker CE, Cheng SH, Parenzan A, Sun YP. *Journal of Nanomaterials and Molecular Nanotechnology*, 2012; 1(2).
7. Rajaram P, Goswami YC, Rajagopalan S, Gupta VK. *Materials Letters*, 2002: **54:**158-163.
8. Nagaich S, Goswami YC. *Fifth International Conference on Advanced Computing & Communication Technologies*, 2015; **1:**65-168.
9. Nilavazhagan S, & Muthukumaran S. *Superlattices and Microstructures*, 2015; **83:**507-520.
10. Patil GE, Kajale DD, Shinde SD, Wagh VG, Gaikwad VB, Jain GH. *Advancement in Sensing Technology,* 2013; **1:**299-311.
11. Zhu H, Yang D, Yu G, Zhang H, Yao K. *Nanotechnology*, 2006;**17(9):**2386.
12. Du F, Guo Z, Li G. *Materials Letters*, 2005; **59(19-20):**2563-2565.
13. Parra R, Ramajo LA, Góes MS, Varela JA, Castro MS. *Materials Research Bulletin*, 2008; **43(12):**3202-3211.
14. Wang WW, Zhu YJ, Yang LX. *Advanced Functional Materials*, 2007; **17(1):**59-64.
15. Dai ZR, Gole JL, Stout JD, Wang ZL. *The Journal of Physical Chemistry B*, 2002; **106(6):**1274-1279.
16. Kumar V, Rajaram P, Goswami YC. *Journal of Materials Science: Materials in Electronics*, 2017; **28(12):**9024-9031.
17. Dang HP, Luc QH, Le T. *Journal of Alloys and Compounds*, 2016; **687:**1012-1020.
18. Davar F, Salavati-Niasari M, Fereshteh Z. *Journal of alloys and compounds*, 2010; **496(1-2):**638-6343.
19. He JH, Wu TH, Hsin CL, Li KM, Chen LJ, Chueh YL, Chou LJ, Wang ZL. *Small*, 2006; **2(1):**116-120.
20. Williams G, Coles GS. *MRS Bulletin*, 1999; **24(6):**25-9.
21. Hu JQ, Ma XL, Shang NG, Xie ZY, Wong NB, Lee CS, Lee ST. *The Journal of Physical Chemistry B*, 2002; **106(15):**3823-3826.
22. Muthu Kumaran S, Gopalakrishnan R. *Journal of sol-gel science and technology*, 2012; **62(2):**193-200.
23. Pourfayaz F, Khodadadi A, Mortazavi Y, Mohajerzadeh SS. *Sensors and Actuators B: Chemical*, 2005; **108(1-2):**172-176.
24. Mishra RK, Kushwaha A, Sahay PP. *RSC advances*, 2014; **4(8):**3904-3912.
25. Lee SY, Park BO. *Thin solid films*, 2006; **510(1-2):** 154-158.
26. Turgut G, Sönmez E. S*uperlattices and Micro-structures*, 2014; **69:**175-186.
27. Cho JH, Hwang TJ, Joh YG, Kim EC, Kim DH, Lee KJ, et al. *Applied physics letters*, 2006; **88(9):** 092505.
28. Jin H, Xu Y, Pang G, Dong W, Wan Q, Sun Y, Feng S. *Materials chemistry and physics*, 2004; **85(1):** 58-62.
29. Divya J, Pramothkumar A, Gnanamuthu SJ, Victoria DB. *Physica B: Condensed Matter*, 2020; **588:** 412169.
30. Gürakar S, Serin T. M*aterials Science and Engineering: B*, 2019; **251:**114445.
31. Zhang G, Liu M. *Sensors and Actuators B: Chemical*, 2000; **69(1-2):**144-152.
32. Bisauriya R, Verma D, Goswami Y C, *Journal of Materials Science: Materials in Electronics,* 2018, **29:** 1868-1876.
33. More PS, Khollam YB, Deshpande SB, Date SK, Karekar RN, Aiyer RC. *Materials Letters*, 2004; **58(1-2):**205-210.
34. Hu CX, Wu YS, Wei HY, Shi YC, Wu LL. *Journal of materials science*, 2005; **40(23):**6301-6306.
35. Parthibavarman M, Hariharan V, Sekar C, Singh VN. *Journal of optoelectronics and advanced materials*, 2010; **12(9):**1894.
36. Nachiar RA, Muthukumaran S. *Optics & Laser Technology*, 2019; **112:**458-466.
37. Johari A, Srivastav S, Sharma M, Bhatnagar MC. *Journal of magnetism and magnetic materials*, 2014; **362:**1-6.
38. Burstein, E. *Physical review*, 1954; **93(3):**632.
39. Kumar V, Rajaram P, Goswami YC. *Optik*, 2016; **127:**2490-2494.
40. Zhao C, Gong H, Niu G, Wang F. *Sensors and Actuators B: Chemical*, 2020; **324:**128745.
41. Kumar V, Rajaram P, Goswami YC. *Journal of Materials Science: Materials in Electronics*, 2017; **28(12):**9024-9031.
42. Jiang L, Yuan X, Zeng G, Wu Z, Liang J, Chen X, et al. *Applied Catalysis B: Environmental*. 2018; **221:**715-725.
43. Gahlaut UP, Kumar V, Goswami YC. *Physica E: Low-dimensional Systems and Nanostructures*, 2020; **117:**113792.